

† Electronic Supplementary Information (ESI)

Development and application of ligand-based NMR screening assays for γ -butyrobetaine hydroxylase

A. Khan, R. K. Leśniak, J. Brem, A. M. Rydzik, H. Choi, I. K. H. Leung,† M. A. McDonough, C. J. Schofield* and T. D. W. Claridge

Department of Chemistry, Chemistry Research Laboratory, University of Oxford, 12 Mansfield Road, Oxford, OX1 3TA, United Kingdom.

E-mail: tim.claridge@chem.ox.ac.uk, christopher.schofield@chem.ox.ac.uk;

Fax: + 44 1865 285002, Tel: + 44 1865 275658

+ Current address: School of Chemical Sciences, The University of Auckland, Private Bag 92019, Auckland 1142, New Zealand.

Table of Contents

Figure S1 Monitoring the effect of Mn^{II} in solution on the line shape of GBB and 2OG by 1H NMR.....	2
Figure S2 Monitoring the binding of GBB and 2OG to BBOX by direct ligand observation using CPMG edited 1H NMR.....	2
Figure S3 Measurement of the binding constant (K_D) of GBB to BBOX in the presence of Zn^{II} and 2OG.....	3
Figure S4 Measurement of the binding constant (K_D) of GBB to BBOX in the presence of Mn^{II} and 2OG.....	3
Figure S5 Initial rate profile of BBOX catalyzed GBB hydroxylation into L-carnitine used for the determination of the IC_{50} values of isoquinoline-based BBOX inhibitors.....	4
Figure S6 1H NMR assay dose response curves (IC_{50} values) of the isoquinoline-based inhibitors used in the study.....	5
Modelling methods.....	7
References.....	8

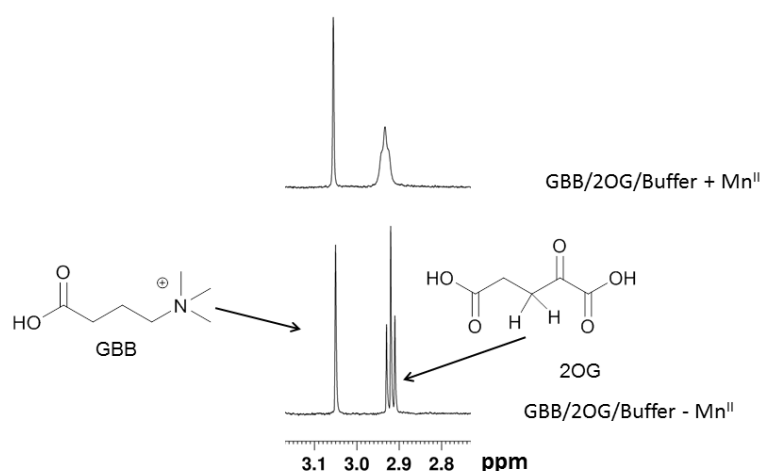


Fig. S1: Monitoring the effect of Mn^{II} in solution on the line shape of GBB and 2OG by 1H NMR (part spectrum shown): Following addition of Mn^{II} , the GBB spectrum is unaffected (singlet at 3.05 ppm), whereas the 2OG triplet (2.91 ppm) is broadened; however the absolute integrated intensity of the latter remains the same with and without Mn^{II} . The final assay mixture contained 25 μM GBB, 300 μM 2OG, 150 μM Mn^{II} , 80 mM KCl, in 50 mM Tris-D11 buffer, pH 7.5, in D_2O .

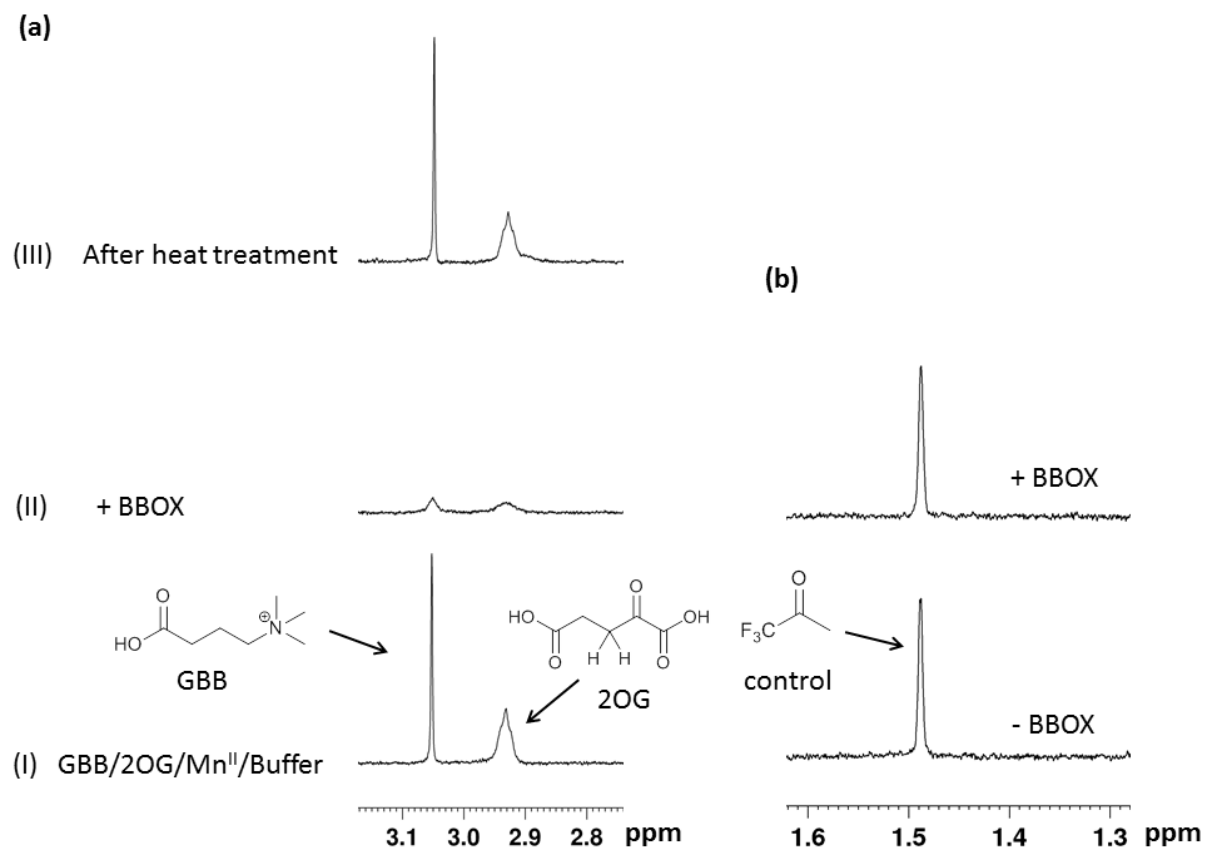


Fig. S2: (a) Monitoring the binding of GBB and 2OG to BBOX by direct ligand observation using CPMG edited 1H NMR (part spectrum shown). (I) GBB/2OG (reporter molecules) with Mn^{II} in buffer. (II) After addition of BBOX (15 μM) to (I); the GBB and 2OG signals are attenuated due to binding with BBOX (III) After heat treatment of (II); denaturation of BBOX results in the recovery of signals for both GBB and 2OG, demonstrating that the signal attenuation/broadening of both these molecules in the presence of BBOX is due to their binding with the protein. (b) Me signal of the 1,1,1 trifluoroacetone (internal NMR control*) in the assay mixture without (bottom spectrum) and with (top spectrum) BBOX. The line-shape of this signal remains the same without and with protein because 1,1,1 trifluoroacetone does not bind BBOX. The final assay mixture contained 25 μM GBB, 300 μM 2OG, 150 μM Mn^{II} , 50 μM 1,1,1 trifluoroacetone as internal NMR control, 80 mM KCl, in 50 mM Tris- D_{11} buffer, pH 7.5, in D_2O .

*NB: 1,1,1 trifluoroacetone is used as a generic standard in our protein binding NMR assays as it proves a convenient for both 1H and ^{19}F NMR.

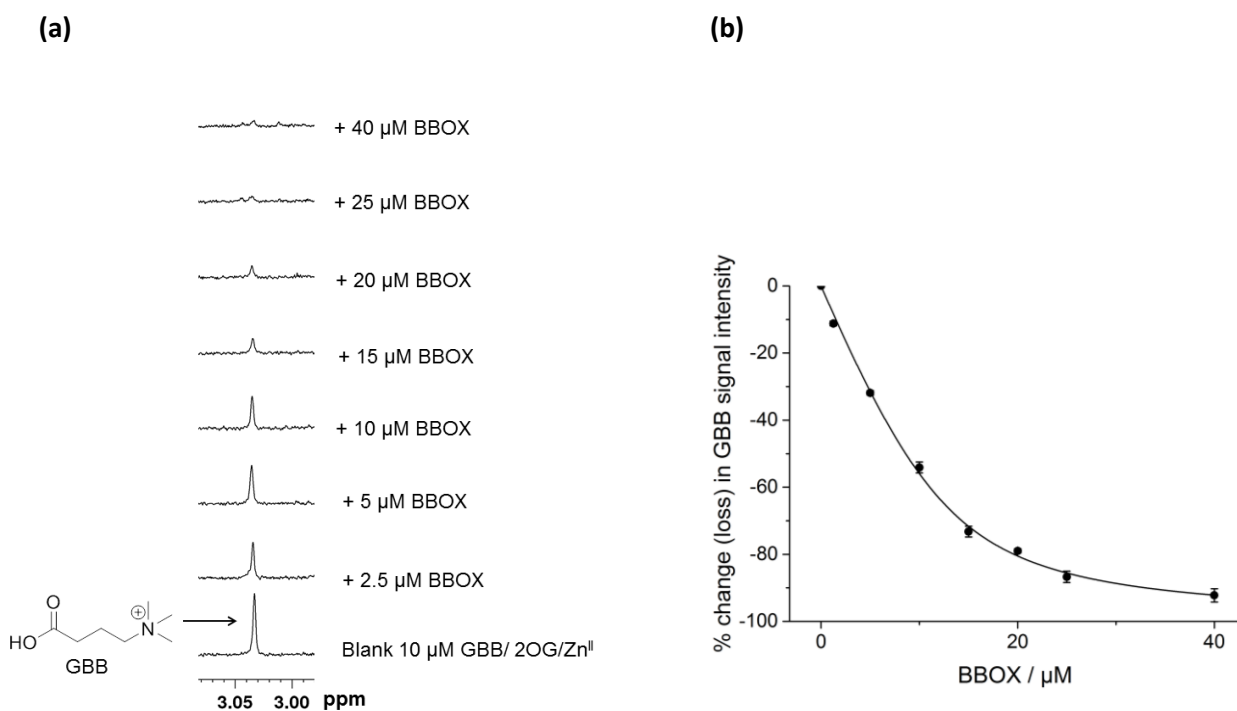


Fig. S3: Measurement of the binding dissociation constant (K_D) of GBB to BBOX in the presence of Zn^{II} and 2OG. **(a)** BBOX titrations to a fixed GBB concentration in the presence of 2OG and Zn^{II} . The loss in GBB signal (Me_3 at 3.05 ppm) intensity is measured as a function of BBOX concentration using a CPMG edited ^1H NMR (part spectrum shown). The final assay mixture contained 10 μM GBB, 300 μM 2OG, 150 μM Zn^{II} , 80 mM KCl, in 50 mM Tris-D11 buffer, pH 7.5, in D_2O . **(b)** Results of the titration data. The K_D obtained is $5 \pm 1 \mu\text{M}$. The error bars represent standard deviations from 3 separate measurements.

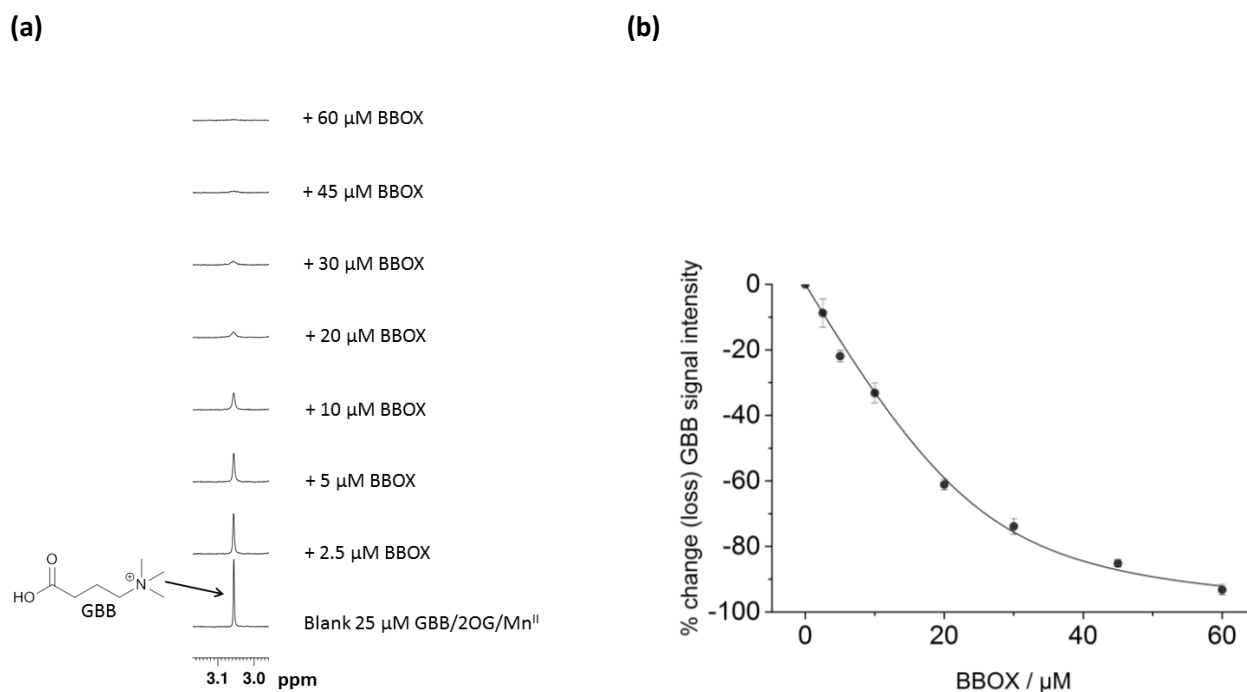
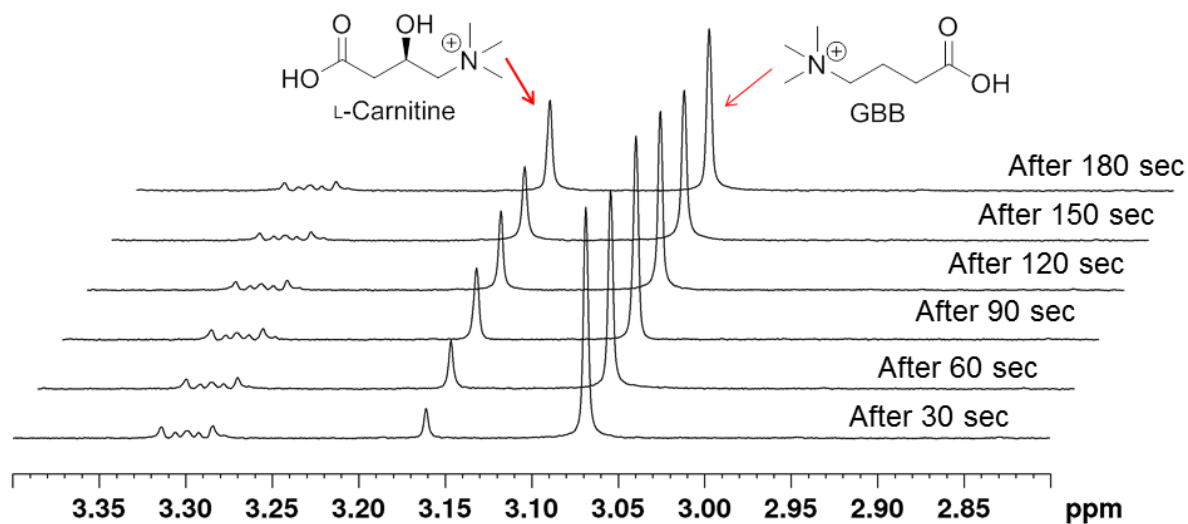


Fig. S4: Measurement of binding constant (K_D) of GBB to BBOX in the presence of Mn^{II} and 2OG. **(a)** BBOX titrations to a fixed GBB concentration in the presence of 2OG and Mn^{II} . The loss in GBB signal (Me_3 at 3.05 ppm) intensity is measured as a function of BBOX concentration using a CPMG edited ^1H NMR (part of the spectra shown). The final assay mixture contained 25 μM GBB, 300 μM 2OG, 150 μM Mn^{II} , 80 mM KCl, in 50 mM Tris-D11 buffer, pH 7.5, in D_2O . **(b)** Results of the titration data. The K_D obtained is $4 \pm 1 \mu\text{M}$. The error bars represent standard deviations from 3 separate measurements

(a)



(b)

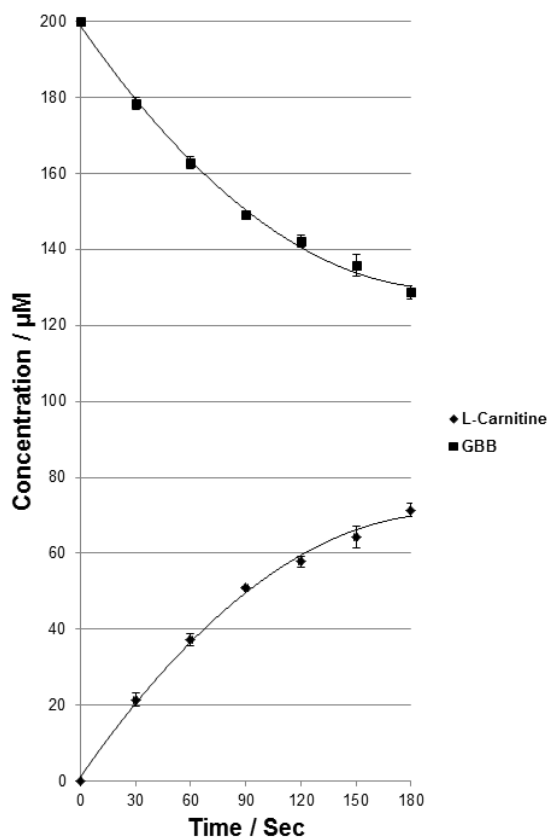
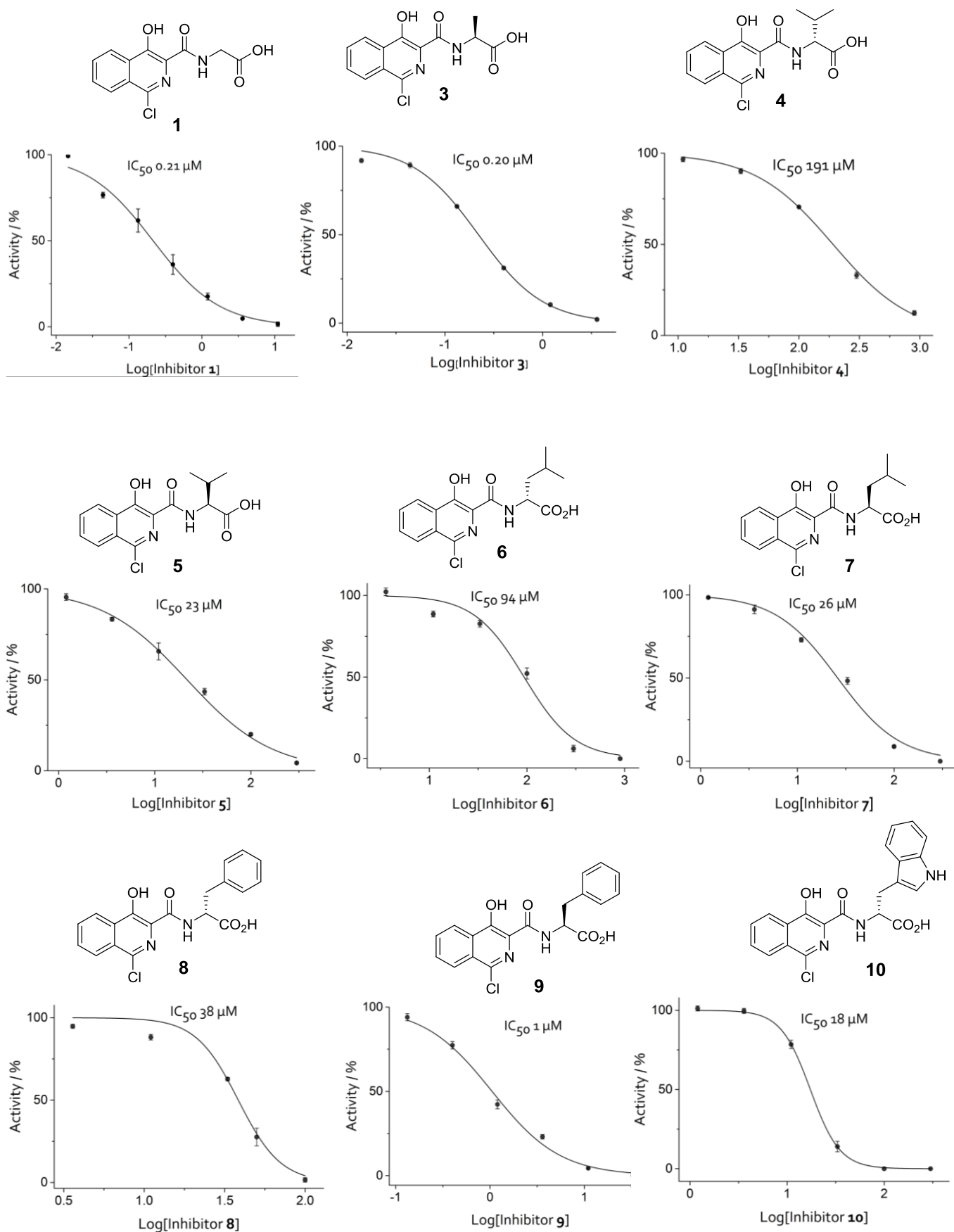
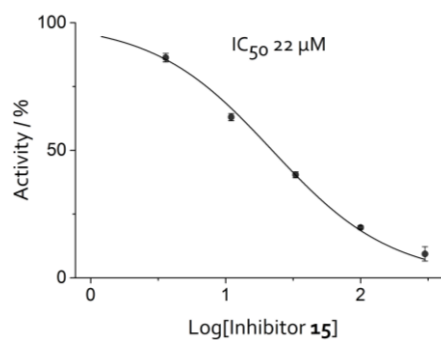
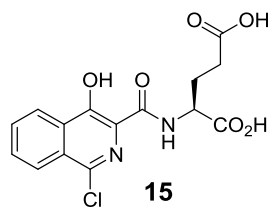
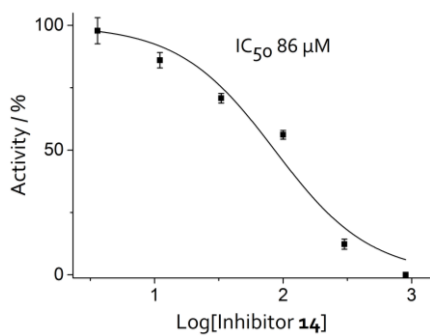
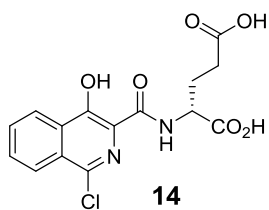
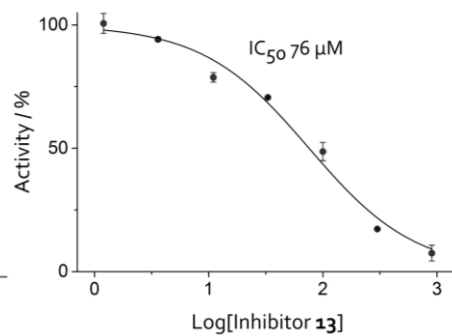
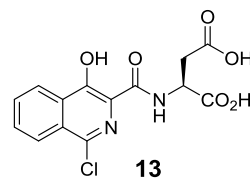
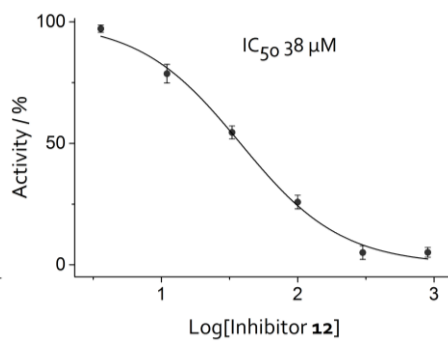
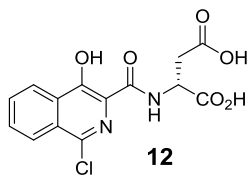
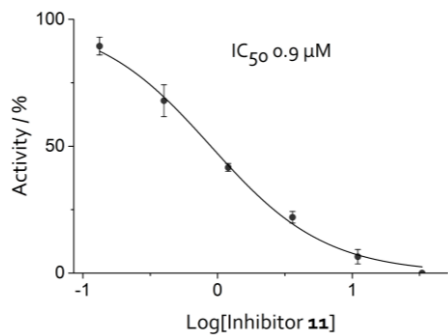
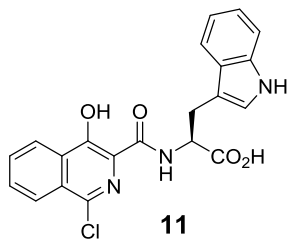


Fig S5: Initial rate profile of BBOX catalysed GBB hydroxylation yielding L-carnitine used for the determination of the IC_{50} values of isoquinoline-based BBOX inhibitors. (a) Overlay of the ^1H NMR spectra (part shown) showing time course analysis of BBOX catalysed GBB turnover to L-carnitine (b) Initial rate profile obtained from the time course data. The reaction was quenched with 10 μL of 1M HCl after 60 s of incubation with BBOX. The final assay mixture contained 200 μM GBB, 600 μM 2OG, 140 nM BBOX, 100 μM Fe^{II} , 500 μM ascorbate and 80 mM KCl in 50 mM Tris-D111, pH 7.5 in D_2O . The error bars represent standard deviations from 3 separate measurements.

Fig. S6: ¹H NMR assay dose response curves (IC₅₀ values) of the isoquinoline-based inhibitors used in this study. The curve for compound 2 is provided in Fig 5b of the main text.





Modelling Methods

For psBBOX1 protein-ligand docking studies, a reported X-ray crystal structure of hBBOX in complex with NOG (unreactive analogue of 2OG), GBB and Zn^{II} (substituent of Fe^{II}) was employed (PDB entry: 3O2G)¹ to make a homology structure of psBBOX using Modeller 9v4.² Attention was paid to the assignment of protonation states for Asp, Glu, His and Lys residues. Atomic charges were then assigned to all the atoms of model of psBBOX through the restrained electrostatic potential (RESP) methods with AMBER program. To address the electronic charge redistribution resulted from the active site Fe^{II} and its ligand groups, we employed the methods involves geometry optimization of simplified model for Fe^{II} in complex with the amino acid residues and well posed ligand 2OG and GBB at B3LYP/6-31** level of theory.³ Table 1 lists the calculated RESP atomic charges of the active site Fe^{II} and its ligand atoms in the optimized structure of the complex. We note that the atomic charge of the Fe^{II} decreases from +2.000 to +1.137 e upon the formation of the complex.

On the other hand, those of the ligand atoms should change the assignment of the atomic charges by means of the RESP method to be consistent with those of psBBOX1; the RESP charge of the nitrogen atom of the two histidine residues is -0.292 and -0.233 respectively, the oxygen of Asp, the two oxygens of 2OG can be assigned -0.630, -0.591 and -0.579 as compared to those in the absence of Fe^{II}. These changes reflect the redistribution of charges between the Fe^{II} and its ligand atoms during the formation of the metal complex, exemplifying that the 'Fe^{II}' model for a metal ion is inadequate for describing the transition metal complexes in the active sites of metalloenzymes. Therefore, we used the newly obtained atomic charges in the potential psBBOX1 inhibitors for docking simulations of small-molecule ligands in the active site of psBBOX1.

Table 1 Calculated RESP charges (in e) of the ferrous ion and its ligand atoms in the model system for psBBOX1-2OG complex

<i>Atoms</i>	<i>RESP charges</i>
Fe	+1.137
His209 NE	-0.292
His350 NE	-0.233
Asp211 OD	-0.630
2OG O2	-0.591
2OG O2'	-0.579

For docking simulations of inhibitor **1** and **11**, the empirical AutoDock⁴ scoring function was used; this was improved by the implementation of a new solvation model for each compound. The modified scoring function has the following form:

$$\Delta G_{bind}^{aq} = W_{vdW} \sum_{i=1} \sum_{j>i} \left(\frac{A_{ij}}{r_{ij}^{12}} - \frac{B_{ij}}{r_{ij}^6} \right) + W_{hbond} \sum_{i=1} \sum_{j>i} E(t) \left(\frac{C_{ij}}{r_{ij}^{12}} - \frac{D_{ij}}{r_{ij}^{10}} \right) \\ + W_{elec} \sum_{i=1} \sum_{j>i} \frac{q_i q_j}{\epsilon(r_{ij}) r_{ij}} + W_{tor} N_{tor} + \Delta G_{sol} = \sum_i^{atoms} \left\{ S_i \left(O_i^{max} - \sum_j^{i \neq j} V_j e^{-\frac{r_{ij}^2}{2\sigma^2}} \right) + P_i \sum_j^{i \neq j} V_j e^{-\frac{r_{ij}^2}{2\sigma^2}} \right\}$$

where W_{vdW} , W_{hbond} , W_{elec} , W_{tor} , and W_{sol} are the weighting factors of van der Waals, hydrogen bond, electrostatic interactions, torsional term, and desolvation energy of the inhibitors, respectively. r_{ij} represents the interatomic distance, and A_{ij} , B_{ij} , C_{ij} , and D_{ij} are related to the depths of the potential energy well and the equilibrium separations between the two atoms. The hydrogen bond term has an additional weighting factor, $E(t)$, representing the angle-dependent directionality. A cubic equation approach was applied to obtain the dielectric constant required to compute the interatomic electrostatic interactions between psBBOX1 and our inhibitors. In the entropic term, N_{tor} is the number of sp^3 bonds in the ligand. In the desolvation term, S_i , P_i and V_i are the solvation parameter, self-solvation parameter and the fragmental volume of atom i , respectively, while Occ_i^{max} is the maximum atomic occupancy.^{5,6}

Reference

1. I. K. H. Leung, T. J. Krojer, G. T. Kochan, L. Henry, F. von Delft, T. D. W. Claridge, U. Oppermann, M. A. McDonough and C. J. Schofield, *Chem. Biol.*, 2010, **17**, 1316-1324.
2. A. Sali and T. L. Blundell, *J. Mol. Biol.*, 1993, **234**, 779-815.
3. J. P. Perdew, K. Burke and M. Ernzerhof, *Phys. Rev. Lett.*, 1996, **77**, 3865-3868.
4. G. M. Morris, D. S. Goodsell, R. S. Halliday, R. Huey, W. E. Hart, R. K. Belew and A. J. Olson, *J. Comput. Chem.*, 1998, **19**, 1639-1662.
5. H. Choi, H. Kang and H. Park, *J. Cheminformatics*, 2013, **5**, 8.
6. H. Kang, H. Choi and H. Park, *J. Chem. Inf. Model.*, 2007, **47**, 509-514.